
Research on Surface Mounting Technology of Micromechanical Silicon Resonant Accelerometer

Libin Huang*, Yang Gao

School of Instrument Science and Engineering, Southeast University, Nanjing 210096, China
Key Laboratory of Micro-Inertial Instrument and Advanced Navigation Technology, Ministry of Education

Corresponding author, e-mail: huanglibin@seu.edu.cn

Abstract

Surface mounting technology is a key process in MEMS packaging. The finite element model of package structures was established in this paper according to the designed micromechanical silicon resonant accelerometer. The effects of package substrate materials, adhesive material characteristics, uneven adhesive thickness, and adhesive defects on the micromechanical silicon resonant accelerometer were analyzed with ANSYS software. Results showed that the package substrate material strongly affected the resonance frequency of the resonator after the application of surface mounting technology. The Young's modulus and thermal expansion coefficient of adhesives were found to be important factors that affect chip thermal stress and warpage. Uneven adhesive thickness and adhesive defects also affect the resonance frequency of the resonator.

Keywords: micromechanical silicon resonant accelerometer, surface mounting technology (SMT), finite element method

Copyright © 2013 Universitas Ahmad Dahlan. All rights reserved.

1. Introduction

Besides the advantages of general MEMS inertial devices, the micromechanical silicon resonant accelerometer has a quasi-digital signal output, easy detection, strong anti-jamming capability, high resolution, and accurate measurement. The accelerometer therefore has good application prospects in fields that demand medium and high accuracy. However, accelerometer development is significantly restricted by the relatively backward MEMS packaging technique.

In published literature, some studies have focused on the structure design, theoretical calculation, processing technology, resonance characteristics of resonant beams, leverage mechanism design, principle prototype development, and the temperature effect of the micromechanical silicon resonant accelerometer [1-17]. Comparatively few studies have focused on the surface mounting technology (SMT) process of a micromechanical silicon resonant accelerometer.

Finite element method was used in this study to analyze the relations among package substrate materials, adhesive material characteristics, uneven adhesive thickness, adhesive defects and thermal stress, warpage, and resonance frequency of the resonator. The aim is to determine the effects of the SMT process on the accelerometer.

2. Working Principle of the Micromechanical Silicon Resonant Accelerometer

Figure 1 shows that the micromechanical silicon resonant accelerometer consists of double-ended tuning fork (DETF) resonators, proof mass, leverage mechanisms, and folded beams. The resonant beam of the accelerometer is connected to one end with fixed support, whereas the other end is connected to the proof mass via a leverage mechanism. When accelerated, the proof mass converts the external acceleration into inertial force. Inertial force is amplified by the leverage mechanism and is applied to the resonant beam to change its resonance frequency. To reduce interference and improve measurement accuracy, two symmetrical distributed DETF structures were used in the accelerometer. When acceleration input exists, one DETF resonator is subjected to tension and its resonance frequency increases, whereas the other is compressed and its resonance frequency is decreased. The value of acceleration can be calculated from the difference in frequencies.

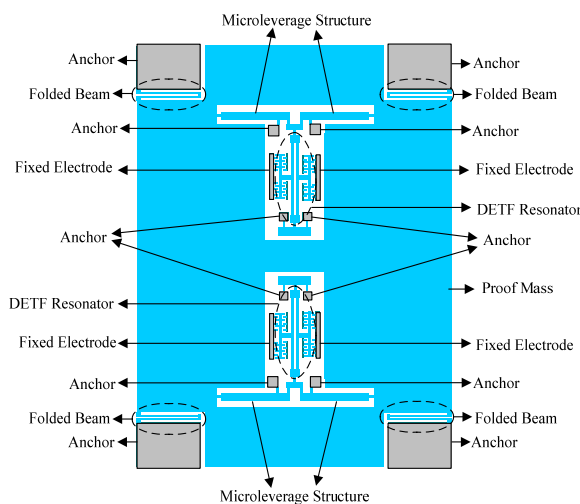


Figure 1. Structure diagram of the micro-mechanical silicon resonant accelerometer.

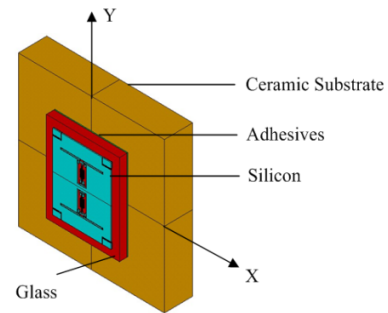


Figure 2. 3-D simulation model of the packaged micromechanical silicon resonant accelerometer.

The resonance frequency of the DETF resonator in axial force is derived from knowledge on vibration mechanics [18] and can be calculated from the following formula:

$$f = f_0 \sqrt{1 \pm F \frac{0.295L^2}{Ehw^3}}, \quad (1)$$

where plus and minus indicate that the resonator suffers from tension and pressure, respectively, F is the axial force, f_0 is the nominal unloaded resonance frequency, and L , w , and h are the length, width, and thickness of the resonator beam, respectively.

When accelerated, the difference output of the accelerometer can be calculated by

$$\Delta f = f_0 \left(\sqrt{1 + F \frac{0.295L^2}{Ehw^3}} - \sqrt{1 - F \frac{0.295L^2}{Ehw^3}} \right) \quad (2)$$

3. Finite Element Simulation of SMT

A micromechanical silicon resonant accelerometer was fabricated with silicon on glass (SOG) process. The accelerometer chip was bonded by silicon and glass material. The SMT process is divided into three steps, namely, glue, SMT, and curing. The SMT structure model can be divided into three layers, namely, the micromechanical silicon resonant accelerometer structure chip, adhesive layer, and substrate. Fig. 2 shows that based on the actual packaged structure of the accelerometer, a simulation model was built with ANSYS software.

3.1. Analysis of the Substrate Material

Metals, ceramics, and PCB substrate are often used as substrate materials of MEMS devices. Table 1 shows the various material parameters of different substrate materials. The adhesive was heated in an 80° C oven according to the actual SMT process. The initial temperature of the entire package structure was set to 80° C during the simulation and then cooled from 80° C to room temperature at 25° C during the solving process. Based on the symmetry of the two resonators, the upper half of the actual model was selected for analysis. The unloaded resonance frequency of the two resonators was obtained as 31263 Hz through simulation analysis of the bare chip without the adhesive layers and the substrate. Table 2 shows the simulation results.

Table 1. Material parameters of package structure

Material	silicon	adhesive	glass	Al ₂ O ₃	AlN	Kovar alloy	FR4	Stainless steel
Young's modulus (Gpa)	130	20	63	307	300	138	16	200
Coefficient of thermal expansion (10 ⁻⁶ □ ⁻¹)	2.6	40	3.25	6.9	3.24	5.6	16	16
Poissons's ration	0.30	0.30	0.20	0.28	0.25	0.37	0.28	0.30

Table 2. Resonant frequency of accelerometer used different substrate material

Substrate material	Al ₂ O ₃	AlN	Kovar alloy	FR4	Stainless steel
Resonant frequency (Hz)	28530	29384	29245	27153	27134

Table 2 also indicates that after the SMT process, a greater reduction in resonance frequency of the resonator than the bare chip was observed regardless of the kind of package substrate material used in the package structure. The thermal expansion coefficient of the ceramic and Kovar alloys is close to the thermal expansion coefficient of the chip material. The resonance frequency variation of the accelerometer with the ceramic and Kovar alloy materials as the substrate is relatively small. During the full temperature test, the temperature characteristics of the accelerometer that used metal material as substrate is not as good as the one that used ceramic material as substrate. Therefore, ceramic material was used as the substrate of the accelerometer. In ceramic materials, the thermal expansion coefficient of AlN material is closer to the thermal expansion coefficient of silicon and glass than the thermal expansion coefficient of Al₂O₃ material. Thus, the use of AlN material as substrate material can reduce packaging thermal stress. However, AlN material is more costly than Al₂O₃ material. Therefore, Al₂O₃ material was used in this study as substrate material in consideration of cost.

3.2. Effects of Adhesive Material Characteristics on Stress and Warpage of the Chip

The Young's modulus and thermal expansion coefficient of adhesives are different with accelerometer chips in the SMT process. This difference causes warpage of the device chip. A large chip warpage can easily result in broken chips or a crack in the adhesive layer edges.

A series of adhesives was used in the simulation. These adhesives have the same coefficient of thermal expansion at $5 \times 10^{-6} / ^\circ\text{C}$ but a different Young's modulus. An assumption was made in the simulation that the Young's modulus of all SMT adhesives will not change with the temperature. The initial temperature of the entire package structure was set to 25° C during the simulation. In the solving process, the package structure was heated from 25° C to 80° C. Figure 3 shows that after extracting the stress at the center of the left beam of the resonator, the relationship between the stress and the Young's modulus was determined. Figure 4 shows the relationship between the warpage of the accelerometer chip and the Young's modulus of the adhesive.

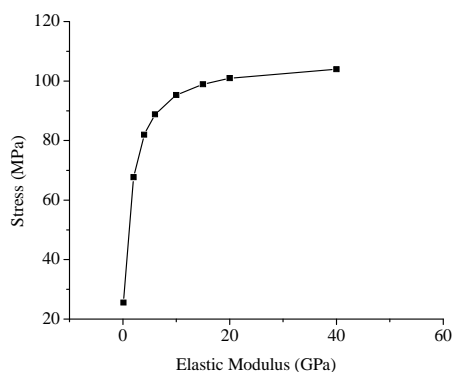


Figure 3. Effect of Young' modulus on thermal stress.

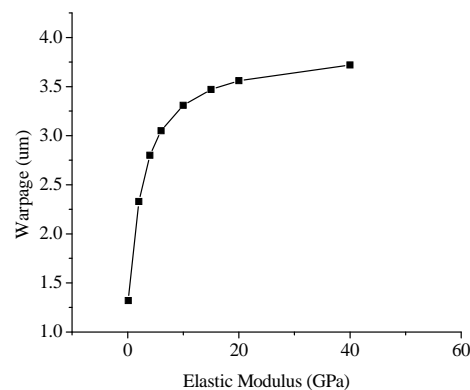


Figure 4. Relation between Young's modulus and warpage.

Figure 3 and 4 show that at a certain range, the higher the Young's modulus, the greater are the inducing stress and warpage. However, when the Young's modulus exceeds a certain value, the stress and warpage slowly increase.

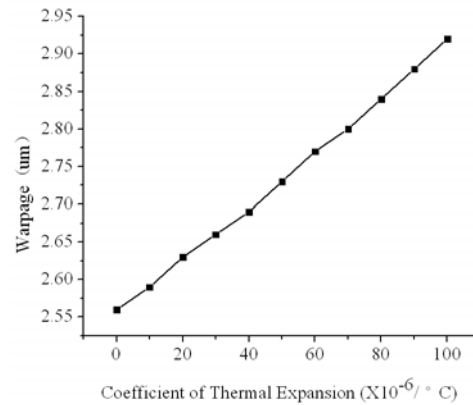
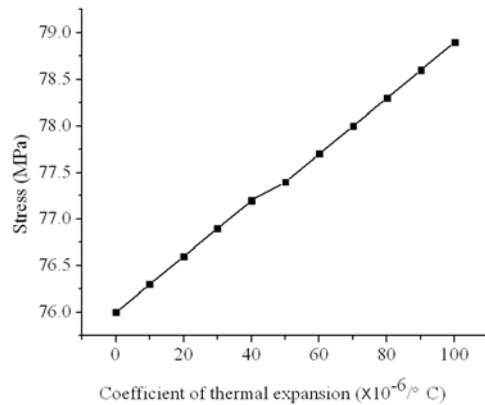


Figure 5. Effects of adhesive's thermal expansion coefficient on the chip's thermal stress

Figure 6. Relation between adhesive's

Suppose all adhesives have the same Young's modulus of 3 Gpa and have different thermal expansion coefficients; Figure 5 shows the relationship between the thermal expansion coefficient and the chip stress. Figure 6 shows the relation curve between the thermal expansion coefficient and the chip warpage. Figures 5 and 6 show that when the temperature is varied, the thermal stress and warpage of the chip increases with an increase in the thermal expansion coefficient.

3.3. Effects of the Uneven Adhesive Thickness

The SMT in MEMS devices is commonly utilized in SMT process equipment for SMT operation. SMT process equipment includes an automatic SMT machine, semi-automatic SMT machine, and manual SMT machine. In actual operation, any one of the SMT machines cannot guarantee the uniform adhesive thickness of the device.

Assume that the adhesive layer gradually thickens along the positive Y-axis direction, and the inclination angle is 1 degree. The stress and strain distribution of the package structure is shown in Figure 7 when the temperature varies from 80 °C to room temperature at 25 °C. Figure 7 shows that the stress acting on the lower resonator is larger than that acting on the upper resonator. The resonance frequency of the lower resonator is 27970 Hz, whereas that of the upper resonator is 28056 Hz. This result is attributed to the different adhesive thickness and the unequal stress acting on the two resonators. The adhesive thickness of the upper resonator is thicker and the stress acting on it is smaller than those of the lower resonator. Thus, the frequency variation in the upper resonator is relatively smaller than that in the lower resonator. Equation (1) shows the ideal case in which no acceleration input exists and the stress acting on the two resonators is exactly the same; the differential output of the accelerometer is zero. The uneven adhesive layer thickness causes the stress acting on the two resonators to differ and the two frequency variations to be unequal. The differential output of the accelerometer will therefore not be zero if no acceleration input exists, and the performance of the accelerometer will be affected.

Assume that the adhesive layer gradually thins along the positive X-axis direction and the inclination angle is 1 degree. Figure 8 shows the stress and strain distribution of the package structure when the temperature varies from 80° C to room temperature at 25° C. Figure 8 shows that the stress acting on the right half of the two resonators is larger than that acting on the left half of the two resonators. The resonance frequency of the lower resonator is 28044 Hz, whereas that of the upper resonator is 28037 Hz. In this case, the adhesive thickness

of the left and right halves of each resonator is not equal, but the adhesive thicknesses of the upper and lower resonators are completely symmetrical relative to the X axis. Thus, the stress acting on the two resonators is equal, and the two frequency variations are the same. If no acceleration input exists, the differential output of the accelerometer will be zero. A difference of 7 Hz exists between the two resonance frequencies because of calculation errors.

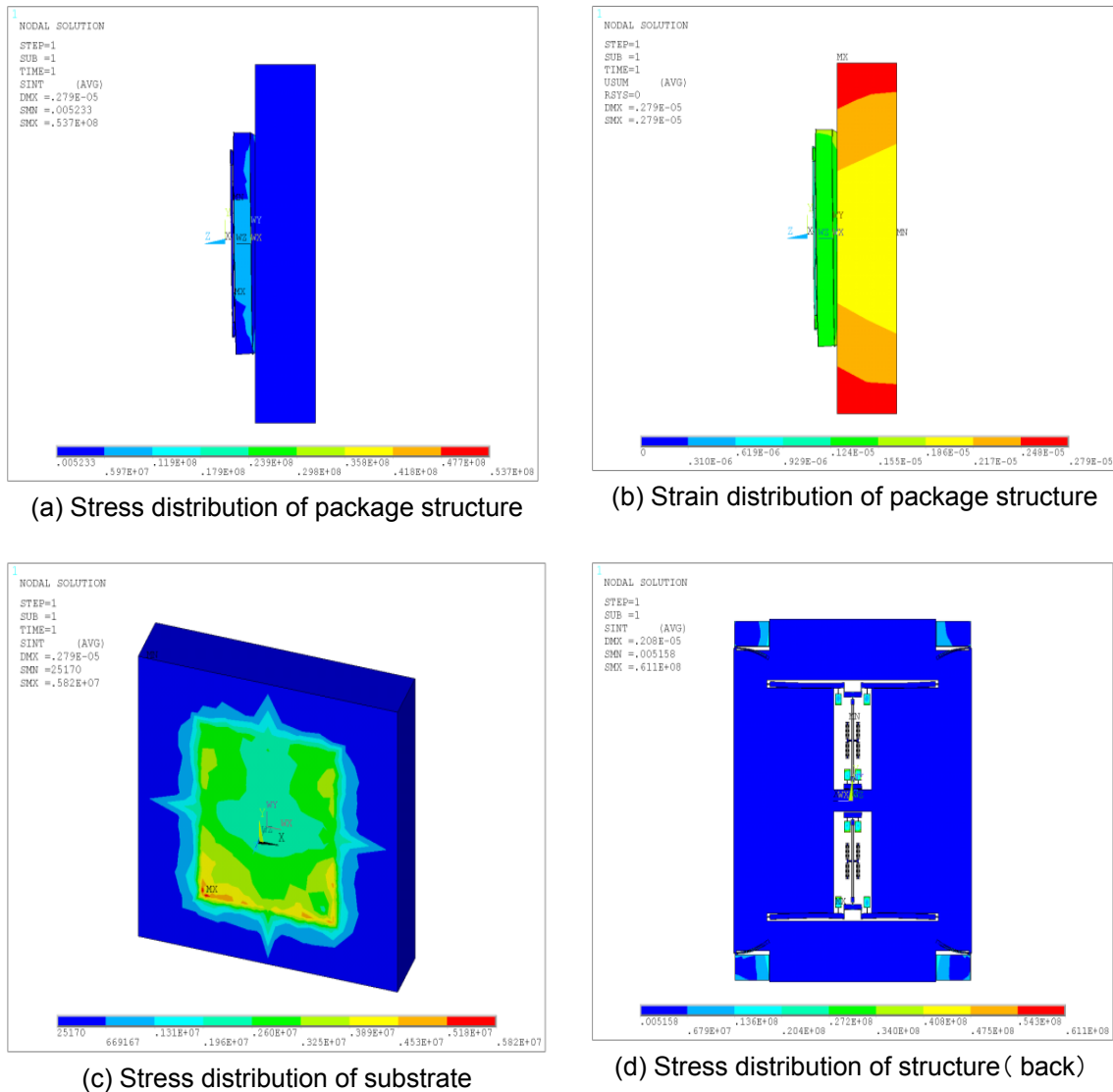
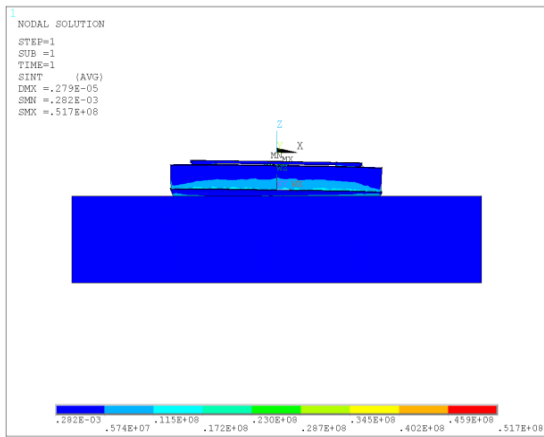


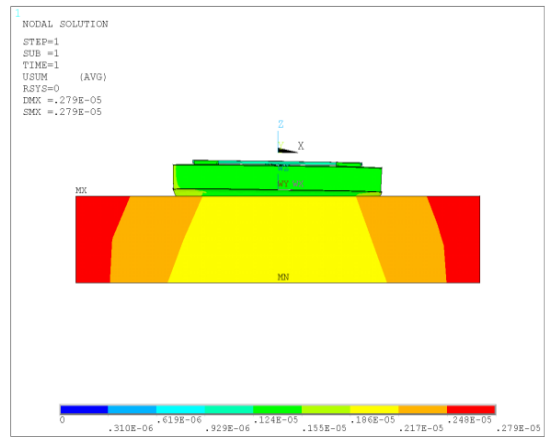
Figure 7. Stress and strain distribution of package structure
(the adhesive layer gradually thickens along the positive Y-axis direction)

3.4. Analysis of Adhesive Defects

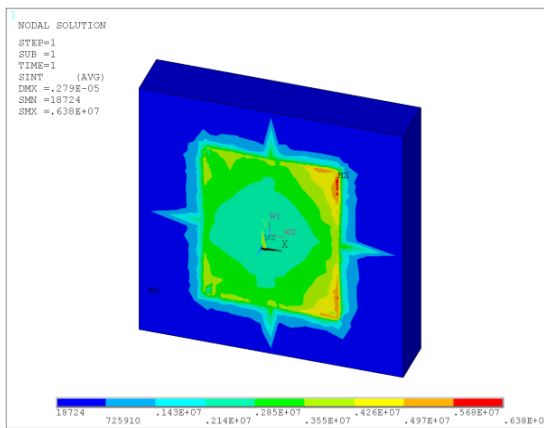
The gas produced in the adhesive curing process or the evaporation of moisture in the SMT process results in bubble holes or other defects in the adhesive layer. Assume that four symmetrically distributed holes are found in the adhesive layer; the stress distribution of the package structure when the temperature varies from 80° C to room temperature at 25° C is as shown in Figure 9. The result indicates that the stress distribution of the two resonators is the same. The resonance frequency of the lower resonator is 28077 Hz, whereas that of the upper resonator is 28084 Hz. With the calculation error ignored, the differential output of the accelerometer is zero.



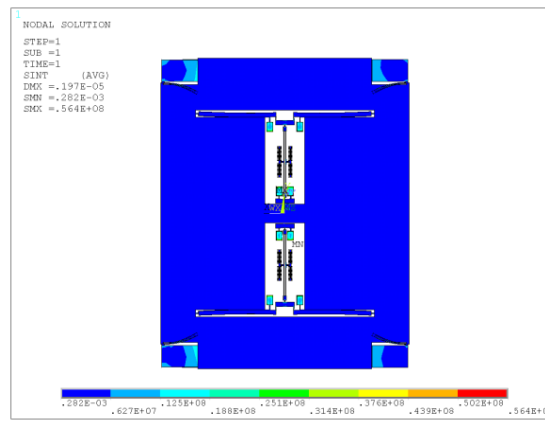
(a) Stress distribution of package structure



(b) Strain distribution of package structure

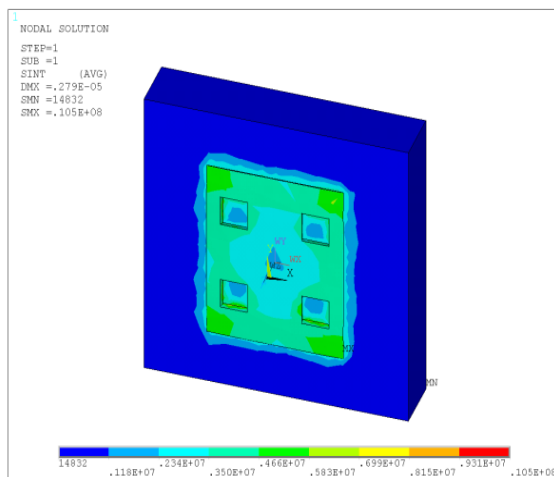


(c) Stress distribution of substrate

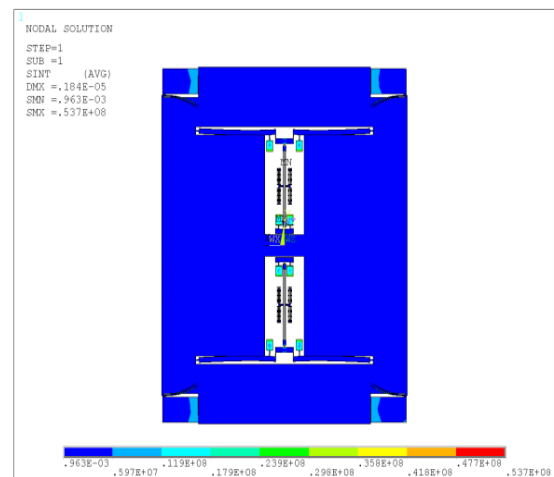


(d) Stress distribution of structure (back)

Figure 8. Stress and strain distribution of package structure (the adhesive layer gradually thins along the positive X-axis direction)



(a) Stress distribution of substrate and adhesive layer



(b) Stress distribution of structure (back)

Figure 9. Stress and strain distribution of package structure (symmetrical defects)

Suppose two holes can be found in the adhesive under the lower resonator, and no defects in the adhesive can be found under the upper resonator; the stress and strain distribution of the package structure when the temperature varies from 80° C to room temperature at 25° C is as shown in Figure 10. The figures show that the stress acting on the lower resonator is larger than that on the upper resonator. The resonance frequency of the lower resonator is 28006 Hz, whereas that of the upper resonator is 28115 Hz. The two frequency variations are unequal. The differential output of the accelerometer is not zero if no acceleration input is found.

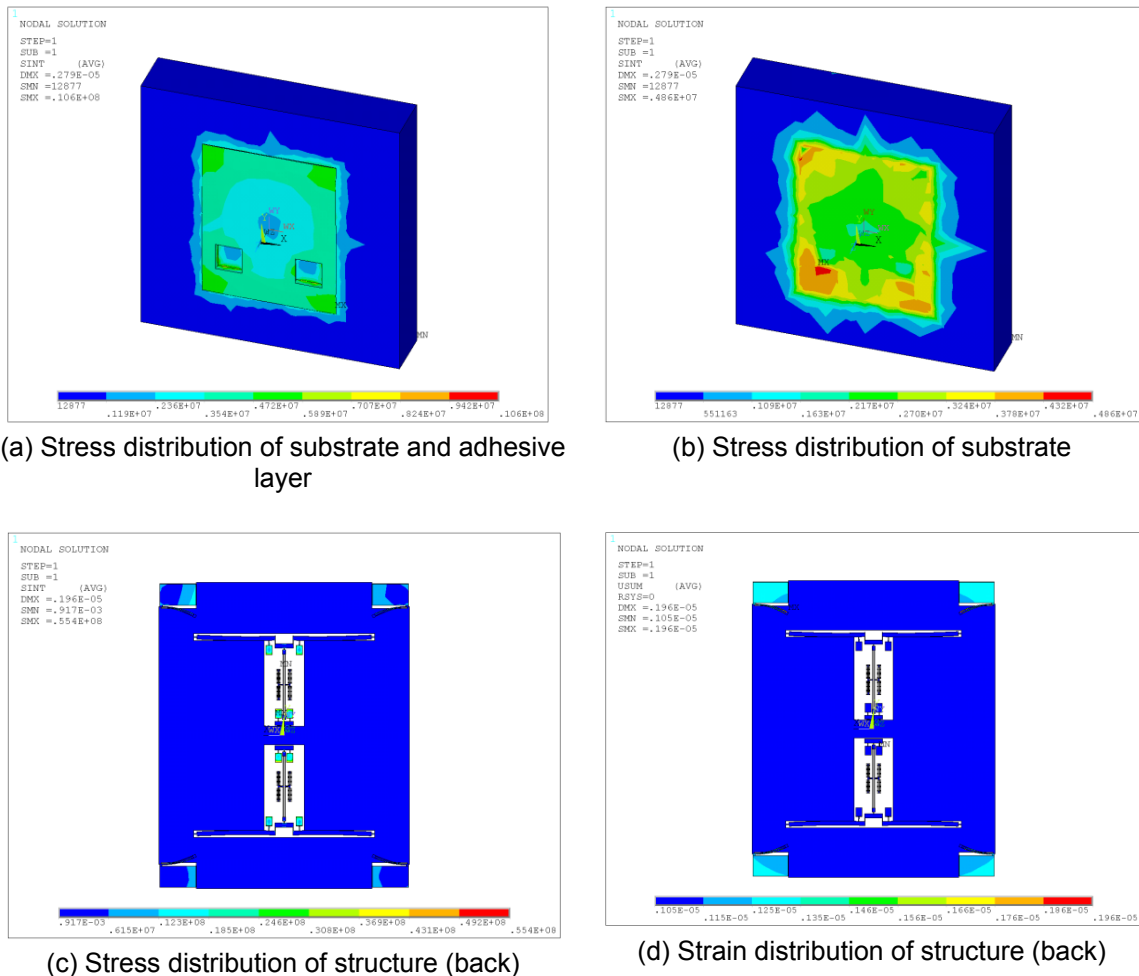


Figure 10. Stress and strain distribution of package structure (asymmetrical defects)

4. Conclusion

The following conclusions can be drawn based on the effects of the SMT process on the micromechanical silicon resonant accelerometer:

- 1) The substrate material of the package structure significantly affects the micromechanical silicon resonant accelerometer. When the thermal expansion coefficients of the substrate material and the chip material are matched, the thermal stress generated after the SMT process is small and has little influence on the resonance frequency of the resonator.
- 2) The Young's modulus and thermal expansion coefficients of the adhesive significantly affect the thermal stress and chip warpage. For the same thermal expansion coefficient, the adhesive of a small Young's modulus can avoid the large thermal stress and chip warpage of the accelerometer when the temperature varies. For the same Young's modulus, the adhesive of the small thermal expansion coefficient is conducive to the reduction in thermal

stress and warpage of the chip.

- 3) Uneven adhesive thickness and defects affect the resonance frequency of the resonator. When the adhesive layer under the two resonators is asymmetrical, the variations in the two resonators are unequal. If no acceleration input can be found, the differential output of the accelerometer will not be zero, and the performance of the accelerometer is affected.

Acknowledgements

This work was supported by the National Natural Science Foundation of China (No. 61101021) and the Jiangsu Provincial Natural Science Foundation of China (No. BK2010401), the Foundation (No. KL201103) of Key Laboratory of Micro-Inertial Instrument and Advanced Navigation Technology, Ministry of Education, China.

References

- [1] Trey A Roessig, Roger T Howe, Albert P. Pisano. *Surface-micromachined resonant accelerometer*. 1997 international Conference on Solid-state Sensors and Actuators. 1997; 859-862.
- [2] Ashwin A Seshia, Moorthi Palaniapan, Trey A Roessig. A vacuum packaged surface micromachined resonant accelerometer. *Journal of Microelectromechanical Systems*. 2002; 11(6): 784-793.
- [3] XPS Su, HS Yang. Single-stage microleverage mechanism optimization in a resonant accelerometer. *Struct Multidisc Optim*. 2001; 21: 246–252.
- [4] Su SXP, Yang HS, Agogino AM. A resonant accelerometer with two-stage microleverage mechanisms fabricated by SOIMEMS technology. *IEEE Sensors Journal*. 2005; 5(6): 1214-1223.
- [5] Kevin A Gibbons. A Micromechanical Silicon Oscillating Accelerometer. M.S. Dissertation. Massachusetts: Massachusetts Institute of Technology; 1997.
- [6] Sangkyung Sung, Jang Gyu Lee, Taesam Kang. Development and test of MEMS accelerometer with self-sustained oscillation loop. *Sensors and Actuators A*. 2003; 109: 1–8.
- [7] Sangkyung Sung, Jang Gyu Lee, Byeungleul Lee. Design and performance test of an oscillation loop for a MEMS resonant accelerometer. *Micromech. Microeng*. 2003; 13: 246–253.
- [8] Hyeon Cheol Kim, Seonho Seok, Ilwhan Kim, et al. *Inertial-grade out-of-plane and in-plane differential resonant silicon accelerometers (DRXLs)*. The 13th International Conference on Solid-state Sensors, Actuators and Microsystems. 2005:172-175.
- [9] Seonho Seok, Hak Kim, and Kukjin Chun. *An inertial-grade laterally-driven MEMS differential resonant accelerometer*. Sensors, 2004. Proceedings of IEEE. 2004: 654-657.
- [10] M Aikele, K Bauer, W Ficker. Resonant accelerometer with self-test. *Sensors and Actuators A*. 2001; 92: 161-167.
- [11] Lin He, Yong Ping Xu, Moorthi Palaniapan. A CMOS readout circuit for SOI resonant accelerometer with 4ug bias stability and 20ug/Hz^{1/2} resolution. *IEEE Journal of Solid-state Circuits*. 2008; 43(6): 1480-1490.
- [12] Christian Burrer, Jaume Esteve, Emilio Lora-Tamayo. Resonant silicon accelerometers in bulk micromachining technology - an approach. *Journal of Microelectromechanical Systems*. 1996; 5(2): 122-130.
- [13] Joshua EY Lee, Behraad Bahreyni, Ashwin A Seshia. An axial strain modulated double-ended tuning fork electrometer. *Sensors and Actuators A: Physical*. 2008; 48(2): 395-400.
- [14] Behraad Bahreyni, Cyrus Shafai. Oscillator and frequency-shift measurement circuit topologies for micromachined resonant devices. *Sensors and Actuators A: Physical*. 2007, 137(1): 74-80.
- [15] PA Hassanpour, WL Cleghorn, E Esmailzadeh, et al. Vibration analysis of micro-machined beam-type resonators. *Journal of Sound and Vibration*. 2007, 308(1-2): 287-301.
- [16] SP Beeby, Graham Ensell, Brian R Baker. Micromachined silicon resonant strain gauges fabricated using SOI wafer technology. *Journal of Microelectromechanical Systems*. 2000, 9(1): 104-111.
- [17] SP Beeby, Graham Ensell, NM White. Microengineered silicon double-ended tuning-fork resonators. *Engineering Science and Education Journal*. 2000; 9(6): 265-271.
- [18] ZH Ni. *Vibration Mechanics*. Xi'an: Xi'an Jiao Tong University press. 1989.